Helical level structure of Dirac potential wells

Daniel Walkup and Joseph A. Stroscio

Phys. Rev. B **96**, 201409 — Published 28 November 2017

DOI: 10.1103/PhysRevB.96.201409

Helical Level Structure of Dirac Potential Wells

Daniel Walkup[1,2†] and Joseph A. Stroscio[1]

[1]Center for Nanoscale Science and Technology, National Institute of Standards and Technology, Gaithersburg, MD 20899, USA
[2]Maryland NanoCenter, University of Maryland, College Park, MD 20742, USA

Abstract

In graphene and other massless 2D Dirac materials, Klein tunneling compromises electron confinement, and momentum-space contours can be assigned a Berry phase which is either zero or π. Consequently, in such systems the energy spectrum of circular potential wells exhibits an interesting discontinuity as a function of magnetic field B: for a given angular momentum the ladder of eigen-resonances is split at an energy-dependent critical field B_c. Here we show that introducing a mass term Δ in the Hamiltonian bridges this discontinuity in such a way that states below B_c are adiabatically connected to states above B_c whose principal quantum number differs by unity depending on the sign of Δ. In the B-Δ plane, the spectrum of these circular resonators resembles a spiral staircase, in which a particle prepared in the $|n, m\rangle$ resonance state can be promoted to the $|n \pm 1, m\rangle$ state by an adiabatic circuit of the Hamiltonian about B_c, the sign depending on the direction of the circuit. We explain the phenomenon in terms of the evolving Berry phase of the orbit, which in such a circuit changes adiabatically by 2π.

† To whom correspondence should be addressed.

Introduction - The light-like carriers in graphene allow optics-inspired analogies such as reflection, refraction, and resonators, to be realized using confining electrostatic potentials and magnetic fields. Tailoring electrostatic p-n junctions have demonstrated geometries with linear boundaries mimicking Fabry-Pèrot etalons [1] and circular p-n junctions have demonstrated the classical analogy of whispering gallery modes [2–4]. A key difference between the wave properties of graphene carriers, and the carriers of conventional two-dimensional electron gases, is the associated chirality and nontrivial Berry phase of the graphene wavefunctions. Chirality and Berry phase in the massless Dirac Hamiltonian describing graphene was recognized in the first experimental papers describing the graphene quantum Hall effect [5,6], and date back to the work in carbon nanotubes [7]. In the Fabry-Pèrot geometry it was shown that the transport conductance underwent a phase shift with the application of a magnetic field, which is traceable to the graphene π Berry phase [8]. More recently, it has been shown that in circular p-n junction geometries, resembling quantum dots (QD), the graphene eigenstates show a discontinuity at a weak critical magnetic field, B_c, which was predicted by theory and confirmed in recent measurements [4,9]. This spectral discontinuity, and its resolution with the addition of a mass term, Δ, is the focus of this work We show in detail that in the three-dimensional space of B, Δ and energy, the spectrum resembles a continuous helical sheet, the successive energy levels of which can be accessed by adiabatic circuits about the discontinuity in B-Δ plane.

The electronic structure of graphene or two-dimensional (2D) Dirac quantum dots has been extensively studied in a wide range of models [10–18]. The arguments given here are applicable to any radially symmetric, monotonic, smoothly varying potential. For concreteness, in the calculations we use a quadratic confining potential, which has been shown to adequately capture the experimental spectrum of graphene QDs measured by scanning tunneling

spectroscopy [2,19], including the Berry phase discontinuity [4]. The helical connectivity of the eigenstate structure is first shown using classical arguments, combined with a consideration of Berry phase. Then, we exhibit the helical spectrum using quantum-mechanical calculations along cuts through the B-Δ plane. Finally, we calculate the eigen-resonances along an elliptical loop surrounding B_c, showing how a picked quantum state would evolve from $|n,m\rangle$ to $|n-1,m\rangle$ along an adiabatic circuit.

Semi-classical analysis- The classical 2D relativistic Hamiltonian for a central potential $U(r)$ can be expressed in polar coordinates as

$$H(r,p_r,\phi,p_\phi) = \pm v_F\sqrt{{p_r}^2 + \left(\frac{p_\phi}{r} - \frac{eB}{2}r\right)^2 + \left(\frac{\Delta}{v_F}\right)^2} + U(r), \quad (1)$$

where v_F is the Fermi velocity, Δ/v_F^2 is the mass, U is the potential energy, and e is the elementary charge. The angular momentum p_ϕ is conserved. For calculations, we take v_F = 10^6 m/s, and $U = \kappa r^2$where $\kappa = 4$ eV/μm^2. The trajectories of Eq. (1) twist at a critical field B_c [9], as shown in Fig. 1(a)-(c). The transition between the left-turning particle [Fig. 1(a)] and the right-turning, looping particle [Fig. 1(c)] involves an intermediate state in which the particle must stop completely and turn back [Fig. 1(b)]. If $\Delta = 0$, we encounter the result that backscattering is forbidden for massless Dirac particles: they do not orbit, but escape the well by Klein tunneling [17,20–22] [Fig. 1(d)]. With finite Δ, however, the classical orbit continues [Fig. 1(e)], and the corresponding quantum states acquire a non-zero lifetime, which can be estimated from the transmission coefficient for Klein-tunneling through a sloped potential barrier. This being $e^{-C\Delta^2}$ [22,23] (where C is a constant that depends on the barrier slope), we see that while at $(B_c, \Delta = 0)$ the eigenstate spectrum must be discontinuous, for finite Δ the

discontinuity is bridged by quasi-bound states [9], whose stability increases super-exponentially with $|\Delta|$. (Hereafter, the $\Delta = 0$ singular point is denoted simply B_c.)

The helical eigenstate structure reported here arises from the fact that these finite-Δ "bridges" connect *different* eigenstates depending on the sign of Δ. This is shown directly in Fig. 3, but can be motived classically by combining the adiabatic theorem [24] with a semiclassical consideration of the Berry phase [9]. Let us start the classical particle in some Hamiltonian [Eq. (1)] defined by (B_0, Δ_0), with arbitrary initial coordinates and momenta, and adiabatically vary B and Δ. In the volume defined by B, Δ, and the energy E, the particle is constrained to move on a sheet defined by the condition $J_r(E) \equiv \oint p_r(r)dr$ = constant. The Berry phase φ_B is included via the modified Bohr-Sommerfeld quantization condition:

$$J_r(E) = 2\pi\hbar\left(n - \frac{\varphi_B}{2\pi} + \gamma\right), \tag{2}$$

where n is the radial quantum number and γ is a constant, here equal to ½ [25,26]. A consistent semiclassical method for calculating φ_B in this system is given in Ref. [9], and summarized below: The quantum Hamiltonian $H = v_F\boldsymbol{\Pi}\cdot\boldsymbol{\sigma} + \Delta\sigma_z + U(r)$ (where $\boldsymbol{\Pi}$ is the kinematic momentum and $\boldsymbol{\sigma}$ the Pauli matrices) has a monopole Berry curvature field $\boldsymbol{\Omega}(\mathbf{h}) = \frac{1}{2}\mathbf{h}/h^3$, where $\mathbf{h} = (\Pi_x, \Pi_y, \Delta/v_F)$. To each classical orbit belongs a closed $\mathbf{h}$-space loop Γ, and φ_B is the flux of $\boldsymbol{\Omega}$ through Γ, in this case one-half the solid angle it subtends [27]. To calculate Γ, one resorts to Einstein-Brillouin-Keller (EBK) quantization [9,28,29]. This procedure defines the action variables J_i as line integrals along the closed surface contours of a phase-space torus. By evaluating $\mathbf{h}$ along the same contours, a closed Γ can be consistently obtained [9]. Further, J_r retains the definition given above, and the resulting φ_B can be directly applied to Eq. (2). Thus it was found that, taking B_c positive and $\Delta = 0$, for $B < B_c$ Γ lies entirely to one side of the origin,

subtending zero solid angle and providing zero Berry phase [Fig. 2(a)], whereas for $B > B_c$ it encircles the origin, providing a Berry phase of π as in the case of pure Landau levels (LLs) [9]. At $\Delta = 0$, the result is a discontinuous jump of the energy levels by half a level, which was observed experimentally [4].

From the above we see that by adiabatically varying B and Δ, we can manipulate Γ to produce an unlimited tunability of φ_B in Eq. (2). Starting for concreteness at an initial Hamiltonian defined by $(B < B_c, \Delta = 0)$, let us see what happens as we attempt a clockwise adiabatic circuit about B_c [Fig. 2]. As we pass over [Fig. 2(b)], down around [Fig. 2(c)], and back underneath the critical point [Fig. 2(d)], we see that Γ (thin blue line) loops over and around the monopole source of Berry curvature in such a way that the solid angle (light blue membrane) increases smoothly from zero in Fig. 2(a) to 4π in Fig. 2(d), so that φ_B grows by 2π. At the classical level, this procedure is fully reversible and repeatable: A second pass over the circuit would make the bubble two layers thick (8π solid angle), a reverse circuit would unwrap one layer of the bubble, and so on. The effect of one circuit is to change the right side of Eq. (2) by $2\pi\hbar$ and, the other terms being constants, the same change must appear in J_r: an adiabatic circuit changes the "effective" radial quantum number by one. Thus when Berry phase is included, the constant-action sheet of the classical particle becomes a connected, multi-level helical manifold in the B-Δ plane, each level of which can be accessed from any other level by repeated circuits about the screw dislocation at B_c.

Quantum simulation and results – To explore this helix structure quantitatively, we performed calculations based on the "spectral method" [30], adapted for 2D Dirac particles. In this procedure, an essentially arbitrary initial wave function $\Psi(\mathbf{r}, 0)$ is evolved numerically under

the time-dependent Schrodinger equation. In general, $\Psi(\mathbf{r},0)$ will have matrix elements with all possible solutions of Schrodinger equation: bound or quasi-bound states, and continuum states. During evolution, the latter quickly propagate to the edge of the simulation area, where they are absorbed, while the former oscillate with their characteristic frequencies $\omega_n = -E_n/\hbar$. These frequencies are extracted post-evolution from the power spectrum of $C(t) \equiv \langle\Psi(0)|\Psi(t)\rangle$, and the eigenstates $\psi(\mathbf{r};E_n)$ are obtained by Fourier-filtering $\Psi(\mathbf{r},t)$ at the corresponding frequency [30]. This enables us to characterize the spectrum of the 2D Dirac Hamiltonian without any *a priori* assumptions, except those which govern the form of the initial wavepacket (see below). Moreover, the inherently dynamic nature of the method allows us to directly enact the adiabatic loops discussed above by evolving a particle, prepared in some eigenstate, in a slowly-varying Hamiltonian .

The time evolution is performed via the third-order [31] split-operator method [32,33], using the 2D Dirac Hamiltonian

$$H(\mathbf{k},\mathbf{r}) = \hbar v_F \begin{pmatrix} 0 & k_x - ik_y \\ k_x + ik_y & 0 \end{pmatrix} + \begin{pmatrix} U+\Delta & -v_F e\left(A_x - iA_y\right) \\ -v_F e\left(A_x + iA_y\right) & U-\Delta \end{pmatrix} \quad (3)$$

where A_x, A_y, and U are functions of $\mathbf{r}$, $\mathbf{k} = \mathbf{p}/\hbar$, and the vector potential is taken in the symmetric gauge. Because the helical spectrum is a property of H at a fixed angular momentum, to obtain it we should choose an initial wavefunction of the form

$$\Psi_m(\mathbf{r},0) = e^{i\left(m-\frac{1}{2}\right)\phi} \begin{pmatrix} u_0(r) \\ e^{i\phi}u_1(r) \end{pmatrix}, \quad (4)$$

where $m\hbar$ is the angular momentum, m is an odd-half integer, and u_0 and u_1 are arbitrary functions containing a broad spectrum of wavelengths. The energies of the spectral peaks are

completely insensitive to the choice of u_0 and u_1 within very broad limits; their amplitudes, however can vary considerably due to matrix element effects. A "good" choice of the u_i provides distinctly nonzero matrix elements with all $|n,m\rangle$ states up to some n_{max}, determined by the shortest wavelength in the u_i, for all (B,Δ) which we wish to study; the spectra of Fig. 3 were obtained with such a function [34].

In Fig. 3 we show resonance spectra of the same initial wave function, for m=5/2, as a function of magnetic field obtained at three characteristic masses less than [Fig. 3(a)], equal to [Fig. 3(b)], and greater than zero [Fig. 3(c)]. As a guide to the eye we include those regions of the (B,E) plane in which classical periodic motion is possible (dark red) or impossible (dark blue), determined by analyzing the function $p_r^2(r)$ extracted from the Hamiltonian in Eq. (1) [34]. For high positive fields [right edge of Fig. 3(a)-(c)] the spectra resemble the well-known quantum Hall energy spectrum: an N=0 LL at energy Δ, which at $\Delta = 0$ bridges the positive and negative LLs whose energies are proportional to $\sqrt{|N|}$. Visually, the movement of this state as a function of Δ is the key to the helix structure. For $\Delta < 0$ the N=0 LL attaches to the group of negative LLs, so that the lowest "positive energy" LL is N=1 [Fig. 3(a)], whereas for $\Delta > 0$ the N=0 state is the lowest positive LL [Fig. 3(c)] [35]. Following our classical discussion, we see that for nonzero mass all the positive-energy states are adiabatically continuous as a function of B: we can re-enact the circuit of Fig. 2 by picking some initial state and sliding along the resonance curves. A brief inspection shows that such a circuit, beginning in state **A** of Fig. 3(b), passes to state **B'** in Fig. 3(c), thence to state **B** in Fig. 3(a) and (b); thus it descends one level of the helix.

To make our picture more complete, we show how the wave functions evolve along a circuit enclosing B_c (Fig. 4). We define the elliptical contour $B = B_0 \cos\theta$, $\Delta = \Delta_0 \sin\theta$ [Fig .4(a)], and in Fig. 4(b)-(l) show how a particular resonance—$n = 1$, $m = 5/2$ in Fig. 4(b)—evolves as a function of θ. For convenience, we use the same adiabatic circuit as in Fig. 2, where θ ranges from π to -π and the state descends the helix by one level, using B_0 = 4 T and Δ_0 = 24 meV. Since the radial motion for fixed m is equivalent to 1D motion in a potential well, let us recall that for the single-component Schrodinger equation, the n^{th} eigenstate is a wave function with n+1 lobes. For these Dirac wells, n can be defined unambiguously only if the lowest positive state is independent of Δ (i.e. for $B < B_c$), and here the "Schrodinger pattern" is followed, in the sense that both components of the Dirac spinor have n+1 radial lobes [Figs. 4(b,l)]. By contrast, for $B > B_c$ (where $\varphi_B \approx \pi$ and n is ill-defined) the wave functions follow the usual pattern of massless Dirac LLs [36], where the upper component has one more radial lobe than the lower [Fig. 4(g)] [37]. These LLs can thus be regarded as "half-integer" states, midway between consecutive equal-lobed states with $\varphi_B = 0$.

As we descend the helix, the resonance gradually sheds its outer lobes. In the first half of the circuit [Fig. 4(b)-(g)], the upper spi [34]nor component becomes stronger (as expected for Δ>0), while the lower components's outer lobe fades in intensity and finally disappears, leaving at θ=0 the standard LL-type eigenspinor [Fig. 4(g)]. Returning with negative Δ [Fig. 4 (h)-(l)], the upper component weakens and similarly loses its outer lobe, so that the resulting state [Fig. 4(l)] has one less lobe in each component. For the circuit shown here, the lobe-fading occupies a fairly narrow range of angles [Figs. 4(d),(e);(i),(j)] corresponding to the condition $B \approx B_c$; we find empirically that the rate of "lobe-shedding" (or adding) along the loop is the more rapid, the shorter is the lifetime of the instantaneous resonance [34].

The process depicted in Fig. 4, in which the particle passes adiabatically between what we would normally regard as *different* eigenstates, deserves some discussion in connection with the quantum-mechanical adiabatic theorem [38,39]. For the quadratic confining potential used here, it was shown [18,34] that throughout the B-Δ plane, the "eigenstates" have the character of resonances with finite lifetimes, to which the theorem does not strictly apply. At high $|B|$, however, the potential could be turned off, and the states would revert to the well-known LLs of the symmetric gauge [36,37]. Then, by turning on the confining potential temporarily together with Δ, we could pass adiabatically to the next higher or lower LL by encircling B_c. This would still not break the adiabatic theorem, since at B_c the confining potential introduces a lifetime of the order e^{Δ^2}: the circuit necessarily passes through a region in which the theorem is inapplicable. The adiabatic time-scale could be much shorter than the lifetime, however [27,40,41], and in an experiment (if feasible), all but an exponentially small fraction of particles might traverse the circuit successfully.

In conclusion, we have shown that the resonance manifold of the 2D Dirac equation in a magnetic field and a smooth central potential, instead of consisting of a series of absolutely separated orthonormal states, is topologically defective: It is subtly linked together so that by turning on a mass term and cycling the sign of the field, a particle in one state can be adiabatically promoted level by level up a helical ladder, or downwards until it reaches at the bottom a state adiabatically connected to the N=0 LL. A direct experimental exploration of this helix requires a method to independently vary Δ and B, which is experimentally challenging. Possible methods to access Δ in graphene include strain engineering [42], or utilizing moiré superlattice potentials [43,44]. More exotic experimental environments might be sought in cold atom systems [45,46] or collections of mechanical oscillators [47]. Although a direct

experimental exploration of this helix structure may be difficult, the discontinuity at Δ=0 has already been observed in graphene [4], and the physics revealed here is broadly applicable to electron confinement in other 2D Dirac materials.

Acknowledgements:

D.W. acknowledges support under the Cooperative Research Agreement between the University of Maryland and the National Institute of Standards and Technology Center for Nanoscale Science and Technology, Grant No. 70NANB10H193, through the University of Maryland. We thank Michael Zwolak, Mark Stiles, and Joaquin Rodriguez-Nieva for valuable discussions.

Figure Captions:

Figure 1: **Classical trajectories near B_c. (a)-(c)** Calculated trajectory of a massless, upward-moving particle released at X=200 Å in magnetic fields slightly less than **(a)**; equal to **(b)**, and greater than **(c)** the critical magnetic field. In (b) the particle escapes by Klein tunneling. **(d), (e)** show the role of the mass in keeping the motion periodic at $B = B_c$: massless particles Klein-tunnel out of the potential well (d), while massive particles remain inside and continue to orbit (e). If the Hamiltonian is varied adiabatically, the path **(f)** must avoid B_c.

Figure 2:**Adiabatic circuit of the Hamiltonian about B_c.** Panels **(a)-(d)** schematically show the momentum-space contour Γ (thin blue ring), the monopole source of Berry curvature $\boldsymbol{\Omega}$ at the origin, and the solid angle subtended by Γ (light blue sheet). During an adiabatic circuit the ring is pulled over the monopole, and the Berry phase increases by 2π. **(e)**, center, shows the circuit in the B-Δ plane, with the locations of panels **(a)-(d)** indicated by red dots. The direction of the adiabatic loop is indicated by green arrows.

Figure 3*:* Screw dislocation in the m=5/2 eigenstate manifold. Panels **(a)**,**(b)**,**(c)** show the resonance spectrum of an m=5/2 wavepacket (see main text) as a function of magnetic field for Δ=-24 meV, 0, and +24 meV respectively. Superimposed on the spectrum (dark-bright color scale) are the regions of phase space where classical periodic motion is possible (red) or impossible (blue) as determined by analysis of the classical Hamiltonian [34].

Figure 4: Evolution of a resonance along an adiabatic loop. (a) In the B-Δ plane we define the elliptical contour $B = B_0 \cos\theta$, $\Delta = \Delta_0 \sin\theta$, where B_0=4 T and Δ_0=24 meV (for other parameters of the Hamiltonian see main text). An adiabatic circuit, identical to that schematized in Fig. 2e, begins at state **A (b)** and proceeds clockwise, arriving at state **B (l)**. The calculated wave functions at intermediate angles are shown in **(c)-(k)**. At positive mass and increasing field (c)-(f), the lower component loses its outer lobe; at negative mass in decreasing field (h)-(k), the upper component loses its outer lobe. In (b)-(l) the subpanel side length is 330 nm; the upper and lower spinor components are shown in the corresponding subpanels. The resonance spectrum as a function of θ is shown in **(m)**, with the path from A to B traced by green arrows.

References:

[1] A. V. Shytov, M. S. Rudner, and L. S. Levitov, Phys. Rev. Lett. **101**, 156804 (2008).
[2] Y. Zhao, J. Wyrick, F. D. Natterer, J. F. Rodriguez-Nieva, C. Lewandowski, K. Watanabe, T. Taniguchi, L. S. Levitov, N. B. Zhitenev, and J. A. Stroscio, Science **348**, 672 (2015).
[3] N. M. Freitag, L. A. Chizhova, P. Nemes-Incze, C. R. Woods, R. V. Gorbachev, Y. Cao, A. K. Geim, K. S. Novoselov, J. Burgdörfer, F. Libisch, and M. Morgenstern, Nano Lett. **16**, 5798 (2016).
[4] F. Ghahari, D. Walkup, C. Gutiérrez, J. F. Rodriguez-Nieva, Y. Zhao, J. Wyrick, F. D. Natterer, W. G. Cullen, K. Watanabe, T. Taniguchi, L. S. Levitov, N. B. Zhitenev, and J. A. Stroscio, Science **356**, 845 (2017).
[5] K. S. Novoselov, A. K. Geim, S. V. Morozov, D. Jiang, M. I. Katsnelson, I. V. Grigorieva, S. V. Dubonos, and A. A. Firsov, Nature **438**, 197 (2005).
[6] Y. Zhang, Y.-W. Tan, H. L. Stormer, and P. Kim, Nature **438**, 201 (2005).
[7] T. Ando, T. Nakanishi, and R. Saito, J. Phys. Soc. Jpn. **67**, 2857 (1998).
[8] A. F. Young and P. Kim, Nat. Phys. **5**, 222 (2009).
[9] J. F. Rodriguez-Nieva and L. S. Levitov, Phys. Rev. B **94**, 235406 (2016).
[10] M. Ezawa, Phys. Rev. B **76**, (2007).
[11] H. P. Heiskanen, M. Manninen, and J. Akola, New J. Phys. **10**, 103015 (2008).
[12] M. Zarenia, A. Chaves, G. A. Farias, and F. M. Peeters, Phys. Rev. B **84**, (2011).
[13] A. Matulis and F. M. Peeters, Phys. Rev. B **77**, (2008).
[14] J. H. Bardarson, M. Titov, and P. W. Brouwer, Phys. Rev. Lett. **102**, 226803 (2009).
[15] A. Matulis, M. Ramezani Masir, and F. M. Peeters, Phys. Rev. A **86**, (2012).
[16] M. Ramezani Masir, A. Matulis, and F. M. Peeters, Phys. Rev. B **84**, (2011).
[17] H.-Y. Chen, V. Apalkov, and T. Chakraborty, Phys. Rev. Lett. **98**, 186803 (2007).
[18] G. Giavaras, P. A. Maksym, and M. Roy, J. Phys. Condens. Matter **21**, 102201 (2009).

[19] J. Lee, D. Wong, J. Velasco Jr, J. F. Rodriguez-Nieva, S. Kahn, H.-Z. Tsai, T. Taniguchi, K. Watanabe, A. Zettl, F. Wang, L. S. Levitov, and M. F. Crommie, Nat. Phys. **12**, 1032 (2016).
[20] M. I. Katsnelson, K. S. Novoselov, and A. K. Geim, Nat Phys **2**, 620 (2006).
[21] V. V. Cheianov, V. Fal'ko, and B. L. Altshuler, Science **315**, 1252 (2007).
[22] P. E. Allain and J. N. Fuchs, Eur. Phys. J. B **83**, 301 (2011).
[23] F. Sauter, Z. Für Phys. **73**, 547 (1932).
[24] L. Landau,L.D. E. M., *Mechanics*, 3rd ed. (Butterworth-Heinemann, 1982).
[25] D. Xiao, M.-C. Chang, and Q. Niu, Rev. Mod. Phys. **82**, 1959 (2010).
[26] G. P. Mikitik and Y. V. Sharlai, Phys. Rev. Lett. **82**, 2147 (1999).
[27] M. V. Berry, Proc. R. Soc. Lond. Math. Phys. Eng. Sci. **392**, 45 (1984).
[28] A. Einstein, Deutshe Phys. Ges. **19**, 82 (1917).
[29] A. D. Stone, Phys. Today **58**, 37 (2005).
[30] M. D. Feit, J. A. Fleck, and A. Steiger, J. Comput. Phys. **47**, 412 (1982).
[31] A. D. Bandrauk and H. Shen, Chem. Phys. Lett. **176**, 428 (1991).
[32] J. A. Fleck, J. R. Morris, and M. D. Feit, Appl. Phys. **10**, 129 (1976).
[33] A. Chaves, G. A. Farias, F. M. Peeters, and R. Ferreira, Commun. Comput. Phys. **17**, 850 (2015).
[34] See Supplemental Material at [URL] for details of numerical methods and semicalssical analysis.
[35] F. D. M. Haldane, Phys. Rev. Lett. **61**, 2015 (1988).
[36] M. O. Goerbig, Rev. Mod. Phys. **83**, 1193 (2011).
[37] Y.-S. Fu, M. Kawamura, K. Igarashi, H. Takagi, T. Hanaguri, and T. Sasagawa, Nat. Phys. **10**, 815 (2014).
[38] T. Kato, J. Phys. Soc. Jpn. **5**, 435 (1950).
[39] M. Born and V. Fock, Z. Für Phys. **51**, 165 (1928).
[40] M. V. Berry, J. Phys. Math. Gen. **17**, 1225 (1984).
[41] J. Hwang and P. Pechukas, J. Chem. Phys. **67**, 4640 (1977).
[42] F. Guinea, M. I. Katsnelson, and A. K. Geim, Nat Phys **6**, 30 (2010).
[43] D. L. Miller, K. D. Kubista, G. M. Rutter, M. Ruan, W. A. de Heer, M. Kindermann, P. N. First, and J. A. Stroscio, Nat. Phys **6**, 811 (2010).
[44] M. Kindermann, B. Uchoa, and D. L. Miller, Phys. Rev. B **86**, 115415 (2012).
[45] L. Tarruell, D. Greif, T. Uehlinger, G. Jotzu, and T. Esslinger, Nature **483**, 302 (2012).
[46] S. Nakajima, T. Tomita, S. Taie, T. Ichinose, H. Ozawa, L. Wang, M. Troyer, and Y. Takahashi, Nat. Phys. **12**, 296 (2016).
[47] S. D. Huber, Nat. Phys. **12**, 621 (2016).

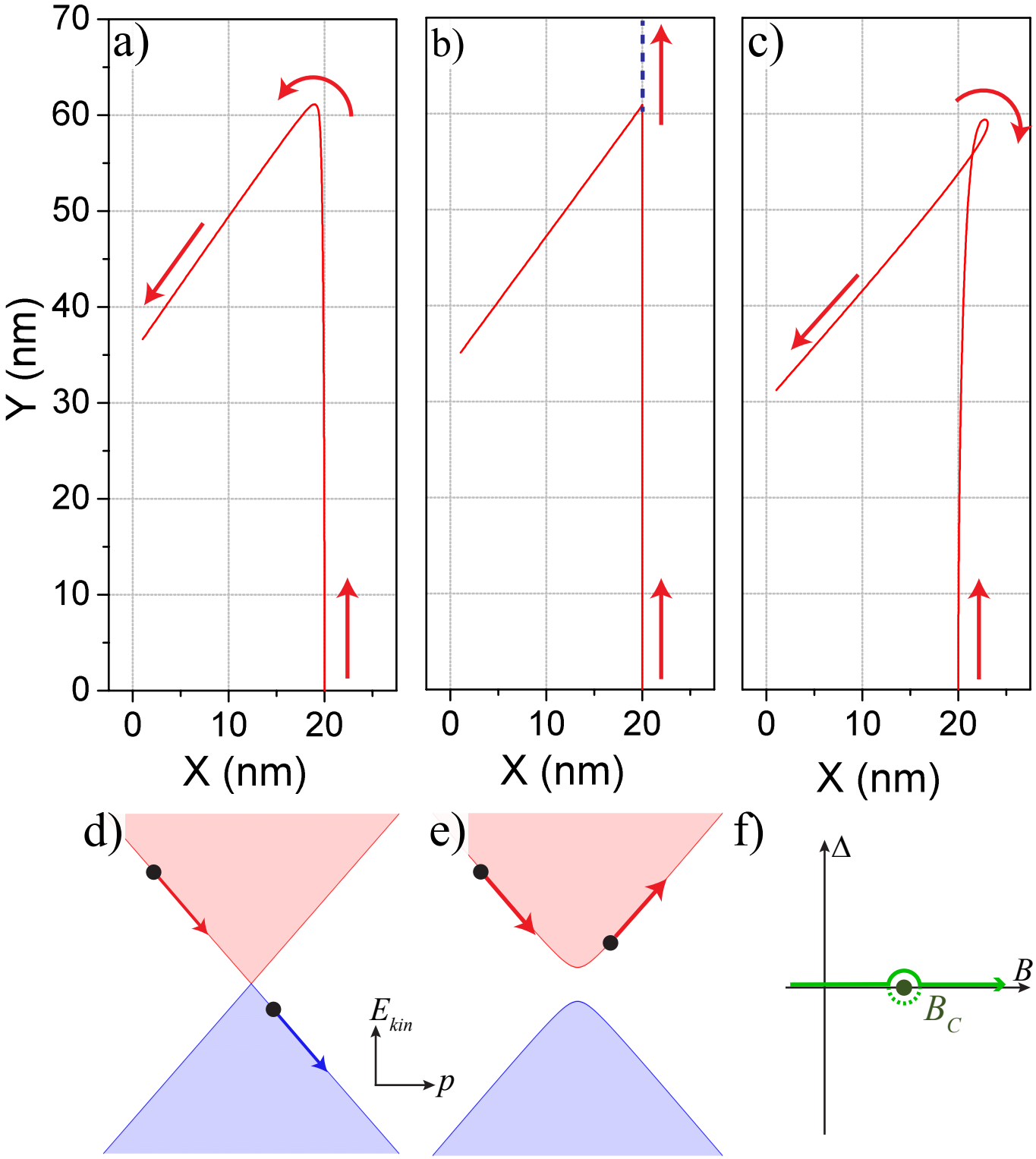

Figure 1

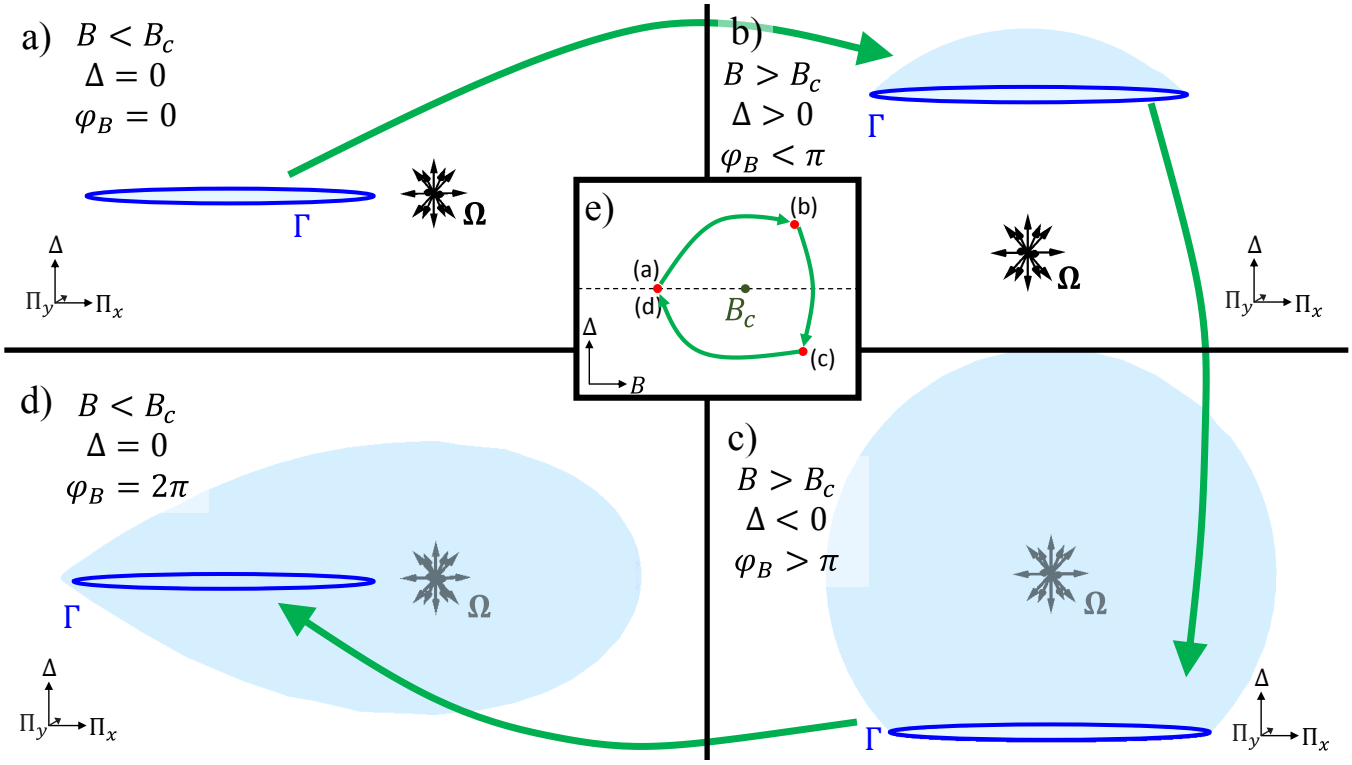
a) $B < B_c$
$\Delta = 0$
$\varphi_B = 0$
b)
$B > B_c$
$\Delta > 0$
$\varphi_B < \pi$
c)
$B > B_c$
$\Delta < 0$
$\varphi_B > \pi$
d) $B < B_c$
$\Delta = 0$
$\varphi_B = 2\pi$
e)
(a)
(b)
(c)
(d)
B_c
Γ
Ω
Π_y
Π_x
Δ
B

Figure 2

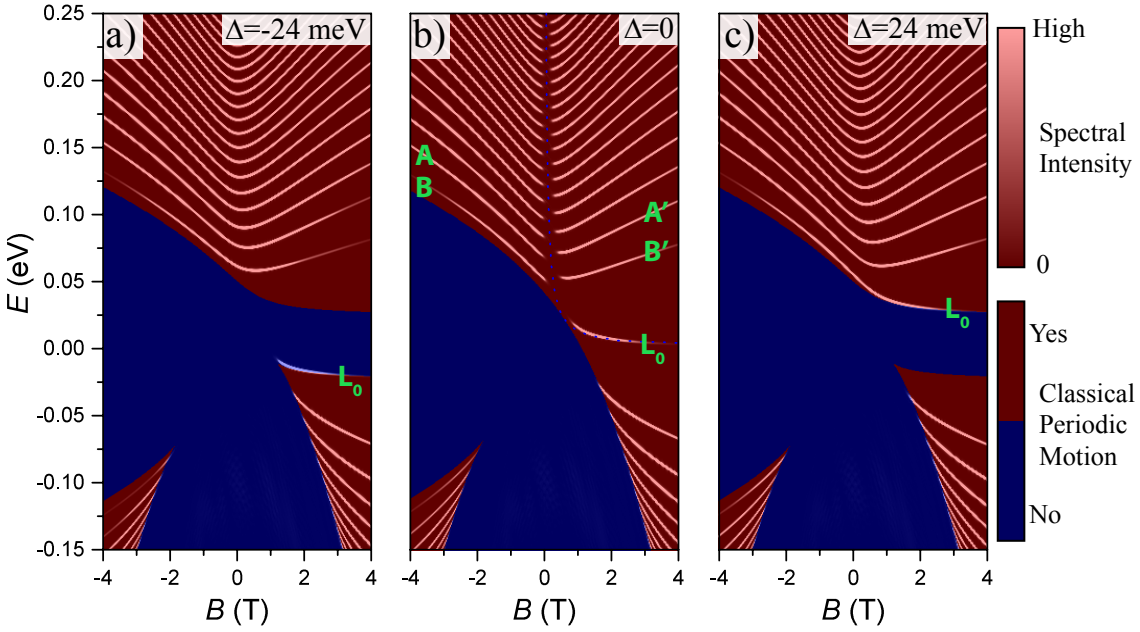
a)
Δ=-24 meV
b)
Δ=0
c)
Δ=24 meV
A
B
A′
B′
L0
L0
L0
E (eV)
B (T)
B (T)
B (T)
High
Spectral
Intensity
0
Yes
Classical
Periodic
Motion
No

Figure 3

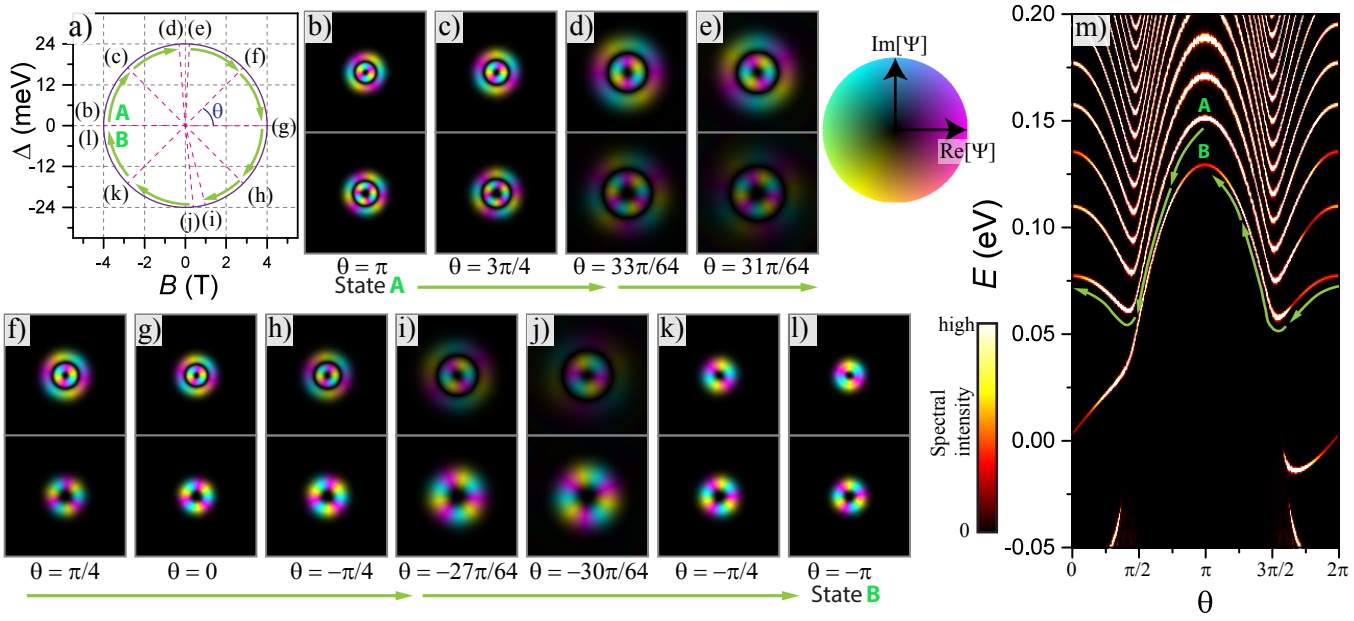
a)
(d) (e)
(c)
(f)
(b)
A
θ
(g)
(l)
B
(k)
(h)
(j) (i)
Δ (meV)
24
12
0
-12
-24
-4
-2
0
2
4
B (T)
b)
c)
d)
e)
θ = π
State A
θ = 3π/4
θ = 33π/64
θ = 31π/64
Im[Ψ]
Re[Ψ]
f)
g)
h)
i)
j)
k)
l)
θ = π/4
θ = 0
θ = −π/4
θ = −27π/64
θ = −30π/64
θ = −π/4
θ = −π
State B
high
Spectral intensity
0
m)
A
B
E (eV)
0.20
0.15
0.10
0.05
0.00
-0.05
0
π/2
π
3π/2
2π
θ

Figure 4